# Fragmentation from spallation of RC slabs due to airblast loads

*by* Ahmad Saiful Haqqi

---

# Fragmentation from spallation of RC slabs due to airblast loads

Chengqing Wu*, Ratni Nurwidayati, Deric John Oehlers

*School of Civil, Environmental and Mining Engineering, The University of Adelaide, North Terrace, South Australia 5005, Australia*

A B S T R A C T

Terrorist attacks using improvised explosive devices on reinforced concrete buildings create a rapid release of energy in the form of a shock wave. Most casualties and injuries resulting from such an attack are not caused by the blast itself, but rather by the disintegration and fragmentation of the RC member due to concrete spallation on the opposite side of the member and which is propelled at high velocities depending on the size of the fragments. Therefore, it is important to analyze the size distributions of the concrete fragments from spallation. In this paper, two RC specimens were tested under explosive loading in a blast chamber: the first, a reinforced concrete (RC) specimen; and the second, an identical RC specimen retrofitted with 6 near surface mounted (NSM) carbon fibre reinforced polymer (CFRP) plates on both the top and bottom faces. Both specimens were subjected to the equivalent 2.1 kg of TNT at a standoff distance of 0.6 m, resulting in significant scabbing of the concrete. All fragments resulting from the blast tests were collected and analyzed. A sieve analysis was carried out to investigate the size distributions of the fragments from the two specimens. It was found that the fragment size followed both a Weibull distribution and a Rosin–Rammler–Sperling–Bennet (RRSB) distribution. The distribution of the fragment shape factor was also studied. The fragment shape factors were distributed according to the lognormal distribution. Furthermore, the influence of fragment size distribution on energy density dissipation was evaluated.

## 1. Introduction

When an explosion is very close to a concrete member, a concrete material behaviour known as scabbing will occur although the concrete member itself may not suffer general failure. Explosion-related injuries and casualties may not result from the blast itself, but rather by the debris discharged from concrete scabbing at high velocities. Blast-induced scabbing of the concrete occurs on the opposite side of the member to the detonation. When the initial compressive shock wave generated by the blast passes through the concrete member and is reflected off the free surface, the shock wave is converted into a tensile wave, resulting in high levels of cracking in the concrete due to its low tensile strength. As the concrete member starts to deflect rapidly, it causes a high-speed discharge of concrete which can become projectile threats to life safety and equipment located on the opposite side of the concrete member, depending on the size of the fragments. Thus, investigation of the size distribution of fragments produced from concrete scabbing due to airblast loads and its effect on dissipated energy density plays an important role in the analysis of fragment threats to life

safety and equipment. However, little information is currently available on the fragments size distribution and energy dissipation through fragmentation from RC specimens under scabbing.

Both experimental and numerical studies have been conducted to investigate scabbing of RC members due to airblast loads [1–8]. For example, spallation damage of reinforced concrete slabs under blast loads was characterized by McVay [1] as: (1) no damage from initial state to a few barely visible cracks; (2) threshold for spallation damage from a few cracks and a hollow sound to a large bulge in the concrete with a few small pieces of spallation on the surface; and (3) moderate spallation damage from a very shallow spallation to spallation penetration up to one third of the plate thickness. Current design guidelines such as TM5 [2,3] on spallation damage of reinforced concrete slabs only provide combinations of estimated explosive charge weights and standoff distances that are likely to generate concrete spallation. Advanced numerical methods such as meshfree methods and finite element methods in recent years have been developed to simulate spallation of reinforced concrete structures subjected to airblast loads [4–8]. Recently, standard concrete cylinders under static loads have been tested to produce fragments and statistical analysis has been conducted to derive fragment size distribution so as to obtain an understanding of the amount of energy dissipated and absorbed through fragmentation [9]. The energy dissipation in crushing and

* Corresponding author. Tel.: +61 8 83034834.
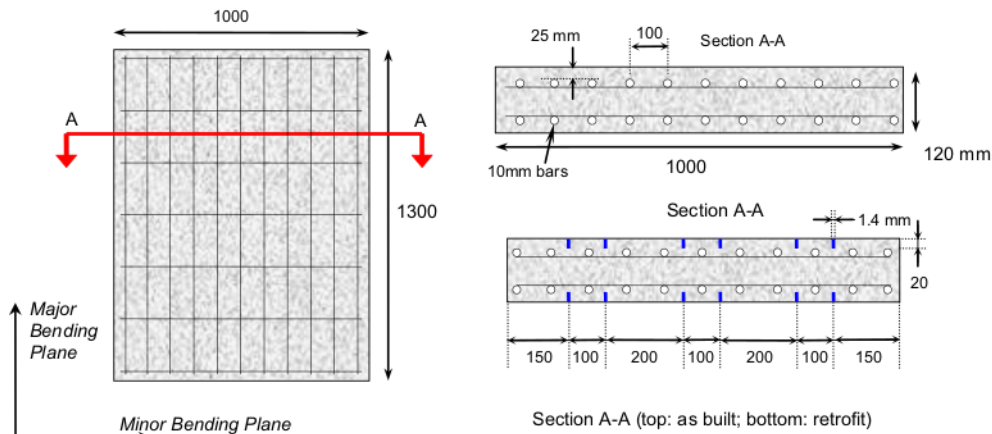*E-mail address:* cwu@civeng.adelaide.edu.au (C. Wu).

**Fig. 1.** Specimens' specifications.

fragmentation has also been investigated based on fragment size distribution [10,11]. However, few studies have been carried out to estimate fragment size distribution resulting from concrete spallation due to airblast loads as well as its influence on energy dissipation governed by the total surface area of the produced fragments.

In this paper, two RC specimens were tested under explosive loading in a blast chamber. The first specimen was an RC slab, while the other was retrofitted with 6 NSM FRP strips on both the top and bottom faces. The specimens were subjected to airblast loads consisting of the equivalent of 2.1 kg of TNT at a standoff distance of 0.6 m. The scabbing holes formed on the opposite face of the two specimens were observed and compared. All the fragments that resulted from concrete scabbing were collected after the blast tests. A sieve analysis was carried out to investigate fragment size distribution and fragment shape factor distribution. It was found that fragment sizes obeyed both a Weibull distribution and an RRSB distribution, and fragment shape factors obeyed a lognormal distribution. The energy dissipated through the spallation of concrete is estimated from the relationship between relative mass and relative size of fragments.

## 2. Blast testing and test results

Two reinforced concrete slab specimens were constructed with the dimensions $1300 \times 1000 \times 120$ mm as shown in Fig. 1. The specimens were reinforced on both the tension and compression faces using a 10 mm diameter mesh with 15 mm of concrete cover. The mesh bars were spaced at 200 mm centres in the major bending plane and 100 mm centres in the minor plane. This represents a reinforcement rate of 0.72%, a typical rate for a reinforced specimen. After curing for 30 days, one specimen was retrofitted with six $1.4 \times 20$ mm NSM CFRP strips spaced across each face of the specimen as shown in Fig. 1 and the retrofit was conducted 15 days prior

to testing. The aggregate size of the concrete was specified at 15 mm. The compressive strength and Young's modulus of the concrete were tested following Australian Standards [12] while the tensile strength was found using the Brazilian Test. The material properties of the test specimens are summarised in Table 1.

Fig. 2 shows the test rig dimensions and the location of the explosive charge in the blast chamber. The test rig provided a simple support for the specimens, however, the upward restraint on the specimens was limited; consequently, wooden chocks were used to assist restraint in the rebound direction. The two specimens were subjected to 2 kg of Comp B, equivalent to 2.09 kg of TNT. Charges were detonated at a standoff distance of 600 mm above the specimen. In order to map the development of scabbing cracks on the primary tension face of the retrofitted specimen, a high-speed camera was used with the aid of the sheet aluminium shields to block light and gas. Fig. 3 shows the scabbing cracks of the retrofitted specimen which were taken using the high-speed photography as the specimen begins to deflect at 3 ms. The scabbing cracks were observed clearly propagating before the gas products occurred. Both specimens experienced scabbing effects under the airblast loads.

**Table 1**
Material properties.

| Material | Young's modulus, $E$ (MPa) | Yield stress, $f_y$ (MPa) | Ultimate Stress, $f_{ult}/f_{rup}/f_{cr}$ (MPa) |
|---|---|---|---|
| Steel mesh | 200 000 | 560 | 605 |
| CFRP | 165 000 | – | 2900 |
| Concrete | 48 000 | – | 48 |



**Fig. 2.** Blast chamber test rig and explosive charge location.

Fig. 3. Scabbing crack at 3 ms.

**Table 2**
Scabbing hole data.

| | Max length (mm) | Max width (mm) | Max depth (mm) | Circumference (mm) | Volume ($\times 10^{-3}$ m³) |
|---|---|---|---|---|---|
| Retrofitted | 670 | 500 | 95 | 2250 | 10.2 |
| Unretrofitted | 600 | 570 | 65 | 2190 | 6.15 |

a smaller average surface area per fragment and more fragments per unit mass of fragmentation.

The interpretation of fragment samples of brittle materials generated from impact, spallation and dynamic fragmentation process is of particular interest. Several equations have been developed to describe the fragments mathematically [13]. One of the most important fragment size distributions is the Weibull distribution suggested by Grady and Kipp [14], which is suitable for handling characteristics of the cumulative distribution of fragment fractions. The cumulative density function is described by

$$P(< D) = 1 - \exp\left[-\left(\frac{D}{D^*}\right)^n\right] \tag{1}$$

where $P(<D)$ is the cumulative weight (in %) of all fragments with diameters smaller than $D$. The parameter $D^*$ is defined as scale parameter, sometimes called as the characteristic diameter which is referred to as the average or maximum diameter of the fragment, and $n$ is shape parameter which is sometimes referred to as the Weibull modulus.

If the analysis is only focused on the fine portion of the grain sample ($D < D^*$), the cumulative weight of all fragments with diameter smaller than $D$ can be approximated as [9]

$$P(< D) = \left(\frac{D}{D^*}\right)^n \tag{2}$$

Then Eq. (2) can be further expressed as follows:

$$\ln P(< D) = \ln\left(\frac{D}{D^*}\right)^n \tag{3}$$

$$\underbrace{\ln P(< D)}_{y} = \underbrace{n}_{a} \underbrace{\ln D}_{x} - \underbrace{n \ln D^*}_{b} \tag{4}$$

By selecting $\ln D$ as the $x$ axis and $\ln P(<D)$ as the $y$ axis, the cumulative Weibull distribution is represented as $y = ax + b$ and the shape parameter $n$ is the slope of the Weibull-distribution function which is graphically estimated. If $D^*$ is referred as the maximum diameter $D_{max}$ of the fragments, the plot of log relative fragment size distributions versus log relative diameter of
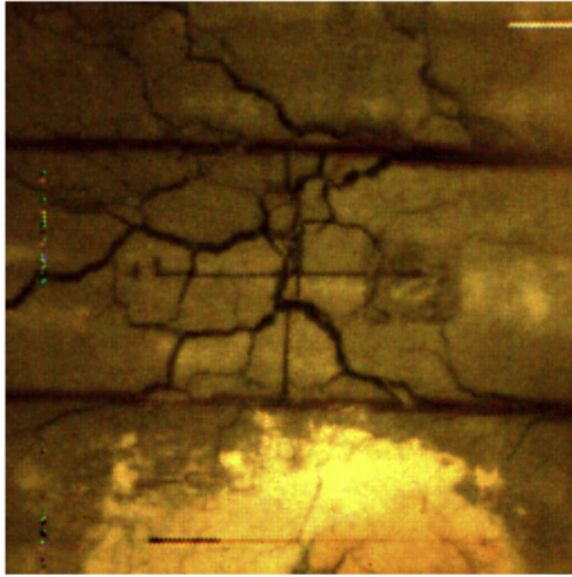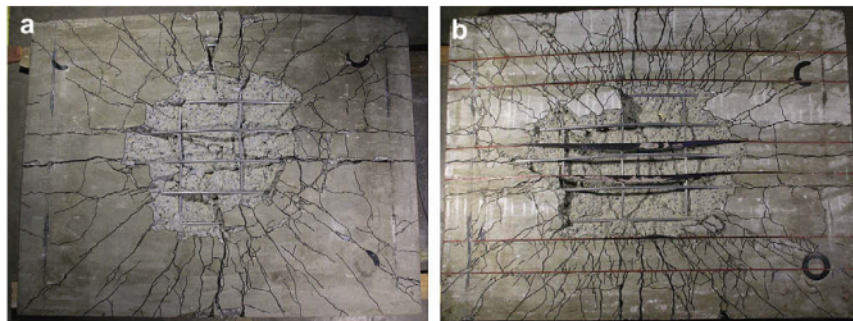
Fig. 4(a) and (b) shows scabbing holes for the two specimens. Table 2 compares the sizes and volumes of the scabbing holes of the two specimens. As shown, the volume of scabbed concrete has increased by over 65% for the retrofitted specimen in comparison with unretrofitted specimen. Though the lengths, widths and circumferences of the scabbing holes in both specimens are comparable, the depth of the scabbing hole in the retrofitted specimen is significantly larger than in the unretrofitted specimen, indicating that NSM retrofitting does not aid in preventing scabbing effects. All fragments were collected after blast tests for sieving analysis.

## 3. Fragment size distribution

The complete samples of fragments for both the retrofitted and unretrofitted specimens were sieved in the laboratory as shown in Fig. 5. In the sieving analysis, the weight of fragments passing through each sieve has been expressed as the percentage of the total weight of the sample. Fig. 6 shows the standard fragment size distribution diagram from the sieve analysis of fragments. As shown, the retrofitted specimen has a higher percentage of smaller fragments than the unretrofitted specimen, indicating that it has



Fig. 4. Scabbing holes in unretrofitted and retrofitted specimens. (a) Unretrofitted specimen (b) retrofitted specimen.

Fig. 5. Samples of fragments from sieving analysis.

fragments for retrofitted and unretrofitted specimens is shown in Fig. 7. From this plot, the slope of the Weibull-distribution function, $n$, is graphically estimated as 0.62 and 0.96 with $R^2$ values of 0.98 and 0.97 for retrofitted and unretrofitted specimens, respectively.

The complete samples of fragments can also be characterized by a Rosin–Rammler–Sperling–Bennet (RRSB) grain-size distribution [13]. The RRSB distribution function is given by Kelly and Spottiswood [13]:

$$\frac{P}{100} = \exp\left[-\left(\frac{D}{D^*}\right)^m\right] \qquad (5)$$

$$\ln\frac{100}{P} = \left(\frac{D}{D^*}\right)^m \qquad (6)$$

$$\underbrace{\text{lnln}\,\frac{100}{P}}_{y} = \underbrace{m}_{a}\,\underbrace{\ln D}_{x} - \underbrace{m\ln D^*}_{b} \qquad (7)$$

Also by choosing $\ln D$ as the $x$ axis and $\text{lnln}(100/P)$ as the $y$ axis, the cumulative RRSB distribution is represented as $y = ax + b$ and the shape parameter $m$ is the slope of the RRSB distribution function. The log–log plot of fragment size distributions versus diameter of fragments for retrofitted and unretrofitted specimens is shown in Fig. 8. From this figure, it can be found that the values of $m$, the slope of the RRSB distribution function, are graphically estimated as 1.15 and 0.91 with $R^2$ values of 0.97 and 0.95 for unretrofitted and retrofitted specimens, respectively.

It should be noted that the Weibull distribution is usually used to present the size distribution of fragments produced by impact and blast loads [14] and the RRSB distribution is suitable for representing the size distribution of fragments induced by quasi-static compressive

loads [13]. However, in this study, since $R^2$ values for both the Weibull distribution and the RRSB distribution are almost the same, indicating both the Weibull distribution and the RRSB distribution are suitable for the description of blast-induced fragments.

## 4. Fragment shape parameter

The fragment shape is estimated by a shape factor which is the ratio of fragment length over its width. The length and width of 200 fragments from each specimen were analyzed by optical microscopy as the fragment lay in its most stable position [15]. Fig. 9 illustrates the histogram of the fragment shape factors for the retrofitted and unretrofitted fragment samples. It can be noted that the unretrofitted specimen tends to have lower shape factors than the retrofitted specimen with respective averages of 1.80 and 1.92. This indicates more uniformity in the fragmentation shape for the unretrofitted specimen. As rounder fragments tend to have a lower surface area than sharp fragments of the same volume, this implies that for a unit mass, fragmentation of the retrofitted specimen will have more crack surface. Since there is a larger surface area per fragment (on average and based on both size and shape factor results) from the retrofitted specimen and also as there was a significantly larger mass of fragmentation recovered (also measured volume) on the retrofitted slab, this points towards notably more force dissipated through the scabbing process for the retrofitted specimen.

As shown in Fig. 9, fragment shape factor $\chi$ may display a lognormal distribution with the probability density function

$$f(\chi) = \frac{1}{\chi\sigma_1\sqrt{2\pi}}\exp\left[-\frac{1}{2}\left(\frac{\ln\chi - \mu_1}{\sigma_1}\right)^2\right] \quad 0 \leq \chi \leq \infty \qquad (8)$$
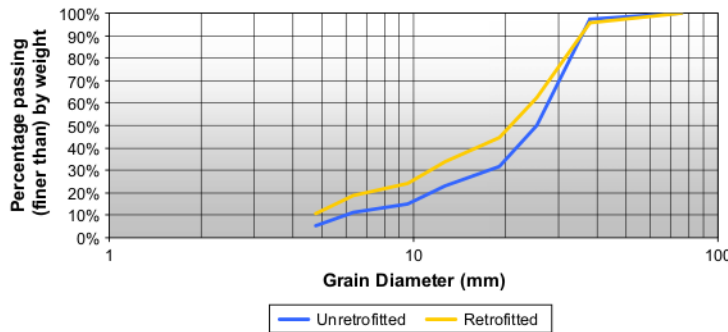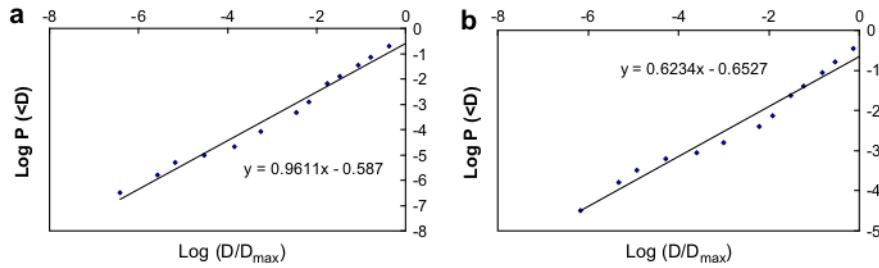


Fig. 6. Sieving analysis of fragments.

**Fig. 7.** Relative size versus relative mass of fragments. (a) Unretrofitted specimen (b) retrofitted specimen.

$$F(\chi) = \Phi\left(\frac{\ln \chi - \mu_1}{\sigma_1}\right) \tag{9}$$

where $\mu_1$ and $\sigma_1$ are the log mean and standard deviation of the shape factor $\chi$ and can be estimated by

$$\mu(\chi) = \exp\left(\mu_1 + \sigma_1^2/2\right) \tag{10}$$

and

$$\sigma^2(\chi) = \mu_1^2(\chi)\left(\exp\left(\sigma_1^2\right) - 1\right) \tag{11}$$

The mean and standard deviation of the shape factor $\chi$ were found to be $\mu(\chi) = 1.92$ and 1.80, $\sigma(\chi) = 0.63$ and 0.53 for the retrofitted and unretrofitted fragment samples respectively. Using Eqs. (10) and (11), the mean $\mu_1$ and standard deviation $\sigma_1$ for the retrofitted and unretrofitted specimens were found to be 0.59 and 0.52, 0.32 and 0.33 respectively. The data for lognormal distributions were also examined by the method of Kolmogorov–Smirnov goodness of fit test technique. It was found acceptable at a confidence level of more than 90% or $\alpha < 0.1$.

## 5. Energy dissipation

It is proposed that energy dissipated through the spallation of concrete can be analyzed as part of the total energy absorbed by the specimen. Momber [9] suggests that debris can give a representation of the amount of energy absorbed and dissipated through the fragmentation cracking process by using the three factors: total weight; size; and shape of fragmentation. Carpinteri and Pugno [16] stated that the energy density is dissipated through producing the new surface and it is proportional to the total surface area of fragments. To estimate the total surface area of fragments, the cumulative density function can also be written as [16]

$$P(<D) = 1 - \left(\frac{D_{\min}}{D}\right)^N \tag{12}$$

The probability density function $p(D)$ times the interval amplitude $dD$ represents the percentage of fragments with diameter comprised between $D$ and $D + dD$. It is provided by derivation of the cumulative distribution function $P(D)$:

$$p(D) = \frac{dP(<D)}{dD} = N\frac{D_{\min}^N}{D^{N+1}} \tag{13}$$

The total surface area of fragments is obtained by integration.

$$
\begin{aligned}
A &= \int_{D_{\min}}^{D_{\max}} f_A(\chi)N_0\left(\pi D^2\right)p(D)dD \\
&= \int_{D_{\min}}^{D_{\max}} f_A(\chi)N_0\left(\pi D^2\right)N\frac{D_{\min}^N}{D^{N+1}}\,dD \cong \frac{f_A(\chi)N\pi N_0}{(2-N)}D_{\min}^N \\
&\quad \times \left(D_{\max}^{2-N} - D_{\min}^{2-N}\right)
\end{aligned}
\tag{14}
$$

where $N_0$ is the total number of fragments and $f_A(\chi)$ is the influence of the shape factor on surface area of fragments. The total volume of the fragments is

$$
\begin{aligned}
V &= \int_{D_{\min}}^{D_{\max}} f_V(\chi)N_0\left(\pi D^3/6\right)N\frac{D_{\min}^N}{D^{N+1}}\,dD \\
&= \frac{f_V(\chi)N\pi N_0}{6(3-N)}D_{\min}^N\left(D_{\max}^{3-N} - D_{\min}^{3-N}\right)
\end{aligned}
\tag{15}
$$

where $f_V(\chi)$ is the effect of the shape factor on volume of fragments. Based on Eq. (15), the mass of fragments with diameters smaller than $D$ is
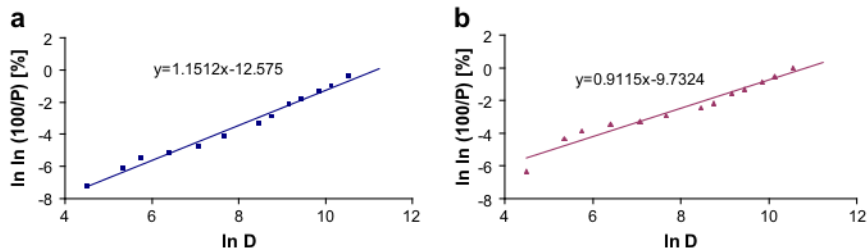


**Fig. 8.** Size distribution of fragments. (a) Unretrofitted specimen (b) retrofitted specimen.
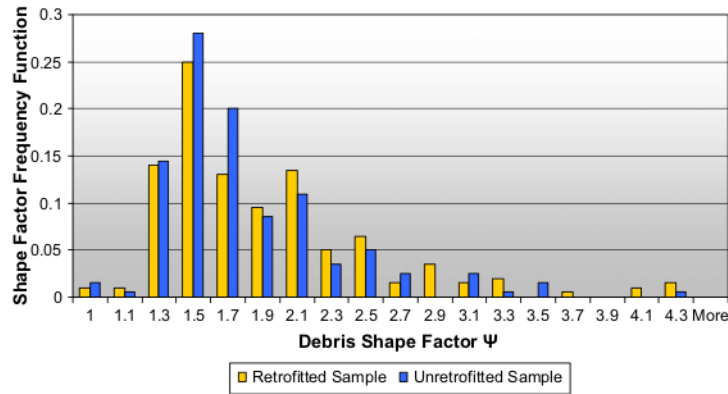
**Fig. 9.** Histogram of fragment shape factor.

$$M(<D) = \frac{f_V(\chi)N\pi N_0\rho_m}{6(3-N)}D_{min}^N D^{3-N} \qquad (16)$$

where $\rho_m$ is material density. Then the ratio of this partial mass to the total mass becomes [10]

$$\frac{M(<D)}{M} \cong \left(\frac{D}{D_{max}}\right)^{3-N} \qquad (17)$$

Since $M(<D)/M = P(<D)$, the exponent $3-N$ in Eq. (17) represents the slope in the bi-logarithmic diagram of relative fragment size distributions versus relative diameter of fragments (i.e. log relative mass versus log relative size of fragments) as shown in Fig. 7. From Fig. 7, it was estimated that $N$ for retrofitted and unretrofitted specimens was 2.38 and 2.04 respectively.

Due to $2 < N < 3$, the energy per unit volume $W$ dissipated during fragmentation, which is proportional to the total surface area $A$ over the total fragmented volume $V$ (i.e. surface area per unit volume), can be estimated by

$$W \propto A/V = \frac{6(3-N)f_A(\chi)}{(N-2)f_V(\chi)}D_{min}^{2-N}D_{max}^{N-3} \qquad (18)$$

Assuming that fragment size $D_{min}$ is a constant [14], $f_A(\chi)$, $f_V(\chi)$ and $N$ are also constants, Eq. (18) can be simplified as

$$W \propto D_{max}^{N-3} \qquad (19)$$

Since $N$ for retrofitted specimen is larger than $N$ for unretrofitted specimen, based on Eq. (19), the energy per unit volume $W$ dissipated during fragmentation for retrofitted specimen is larger than that for unretrofitted specimen, indicating more force dissipated through the scabbing process for the retrofitted specimen.

## 6. Conclusion

Blast testing has been carried out to derive fragment size distribution and fragment shape factor distribution for the unretrofitted and retrofitted RC slabs. By using the method of statistical analysis, it was found that fragment sizes for the unretrofitted and retrofitted RC slabs obey the Weibull distribution, and fragment shape factors obey lognormal distributions. Further to this, it is proposed that energy dissipated through the spallation of concrete can be quantified by the ratio of the total surface area $A$ over the total fragmented volume $V$. It

was found that more energy per unit volume is dissipated during fragmentation for retrofitted specimen in comparison with that for unretrofitted specimen. The statistical analysis in this paper shows considerable potential for gaining a better understanding of the fragmentation from spallation and may possibly become advantageous in the design of scabbing resistant structures. It should be noted that since data involved in the statistical analysis in this research were only collected from two blast tests, the above conclusions might need more testing data for validation.

## References

[1] Mcvay MK. Spall damage of concrete structures. Technical Report SL 88-22, US Army Corps of Engineers Waterways Experiment Station; 1998.
[2] TM5-1300. Structures to resist the effect of accidental explosions. US Department of the Army, Navy and Air Force Technical Manual; 1990.
[3] TM5-855. Design and Analysis of Hardened Structures to Conventional Weapons Effects. Department of Defense, UFC 3-340-01, USA; 2002.
[4] Rabczuk T, Eibl J, Stempniewski L. Numerical analysis of high speed concrete fragmentation using a meshfree Lagrangian method. Engineering Fracture Mechanics 2004;71(4–6):547–56.
[5] Rabczuk T, Eibl J. Simulation of high velocity concrete fragmentation using SPH/MLSPH. International Journal for Numerical Methods in Engineering Mar 14 2003;56(10):1421–44.
[6] Xu K, Lu Y. Numerical simulation study of spallation in reinforced concrete plates subjected to blast loading. Computers and Structures 2006;84:431–8.
[7] Nash PT, Vallabhan CVG, Knight TC. Spall damage to concrete walls from close-in cased and uncased explosions in air. ACI Structural Journal 1995;92(6):680–8.
[8] Zhou XQ, Hao H, Deeks AJ. Modeling dynamic damage of concrete slab under blast loading. In: Hao H, Lok TS, Lu GX, editors. Proceeding of the 6th Asia-Pacific Conference on Shock and Impact Loads on Structures, December, Perth, WA, Australia; 2005. p. 703–10. ISBN: 981–05-3550-3.
[9] Momber AW. The fragmentation of standard concrete cylinders under compression: the role of secondary fracture debris. Engineering Fracture Mechanics 2000;67:445–59.
[10] Carpinteri A, Lacidogna G, Pugno N. Scaling of energy dissipation in crushing and fragmentation: a fractal and statistical analysis based on particle size distribution. International Journal of Fracture 2004;129(2):131–9.
[11] Carpinteri A, Pugno N. Fractal fragmentation theory for shape effects of quasi-brittle materials in compression. Magazine of Concrete Research 2002;54(6):473–80.
[12] AS 3600. Concrete structures, Standards Australia, Homebush, Australia; 2001.
[13] Kelly FG, Spottiswood DJ. Introduction to mineral processing. New York: Wiley; 1982. p. 21–45.
[14] Grady DE, Kipp ME. Dynamic rock fragmentation. In: Atkinson BK, editor. Fracture mechanics of rock. London: Academic Press; 1987. p. 429–75 [chapter 10].
[15] ASTM. Standard test method for compressive strength of cylindrical concrete specimens. Designation: C36-86, New York: ASTM; 1996.
[16] Carpinteri A, Pugno N. A fractal comminution approach to evaluate the drilling energy dissipation. International Journal for Numerical and Analytical Methods in Geomechanics 2002;26(5):499–513.

# Fragmentation from spallation of RC slabs due to airblast loads